

Spectral coherence between climate oscillations and the $M \geq 7$ earthquake historical worldwide record

Nicola Scafetta · Adriano Mazzarella

Received: 4 July 2014 / Accepted: 19 December 2014 / Published online: 1 January 2015
© Springer Science+Business Media Dordrecht 2015

Abstract We compare the NOAA Significant Earthquake Historical database versus typical climatic indices and the length of the day (LOD). The Pacific Decadal Oscillation (PDO) record is mainly adopted because most of the analyzed earthquakes occurred at the land boundaries of the Pacific Plate. The NOAA catalog contains information on destructive earthquakes. Using advanced spectral and magnitude squared coherence methodologies, we found that the magnitude $M \geq 7$ earthquake annual frequency and the PDO record share common frequencies at about 9-, 20-, and 50- to 60-year periods, which are typically found in climate records and among the solar and lunar harmonics. The two records are negatively correlated at the 20- and 50- to 60-year timescales and positively correlated at the 9-year and lower timescales. We use a simple harmonic model to forecast the $M \geq 7$ significant earthquake annual frequency for the next decades. The next 15 years should be characterized by a relatively high $M \geq 7$ earthquake activity (on average 10–12 occurrences per year) with possible maxima in 2020 and 2030 and a minimum in the 2040s. On the 60-year scale, the LOD is found to be highly correlated with the earthquake record ($r = 0.51$ for 1900–1994, and $r = 0.95$ for 1910–1970). However, the LOD variations appear to be too small to be the primary earthquake trigger. Our results suggest that large earthquakes are triggered by crust deformations induced by, and/or linked to climatic and oceanic oscillations induced by astronomical forcings, which also regulate the LOD.

N. Scafetta (✉) · A. Mazzarella
Meteorological Observatory, Department of Earth Sciences, Environment and Georesources,
University of Naples Federico II, Largo S. Marcellino 10, 80138 Naples, Italy
e-mail: nicola.scafetta@unina.it

A. Mazzarella
e-mail: adriano.mazzarella@unina.it

N. Scafetta
Active Cavity Radiometer Irradiance Monitor (ACRIM) Lab, Coronado, CA 92118, USA

N. Scafetta
Duke University, Durham, NC 27708, USA

1 Introduction

Earthquake predictability is one of the most challenging geophysical problems. Earthquakes occur in clusters where usually a large earthquake triggers a number of aftershocks of various magnitude that can trigger other earthquakes giving rise to a local earthquake avalanche. Some studies have suggested that earthquakes could be partially triggered by solar and lunar tidal forces (e.g., Chen et al. 2012; Cochran et al. 2004; Lopes et al. 1990; Mazzarella and Palumbo 1988, 1989; Riguzzi et al. 2010), correlated with climate change phenomena (e.g., Bollinger et al. 2007; Gao et al. 2000; Heki 2003; Liu et al. 2009; Luttrell and Sandwell 2010; McGuire 2013; Miller 2008; Pagli and Sigmundsson 2008; Panza et al. 2011; Saar and Manga 2003; Wu and Johnston 2000) and associated with changes in the length of the day (LOD) (e.g., Mörner 1989, 1998, 2013; Ostřihanský 2012; Riguzzi et al. 2010; Wang et al. 2000). Because astronomical and (partially) climatic oscillations are cyclical (e.g., Klyashtorin et al. 2009; Ogurtsov et al. 2002; Scafetta 2010a, 2012b, 2013b) and approximately predictable using harmonic models at the decadal and multidecadal scales, determining the existence of a link between large earthquake occurrences and astronomical and/or climatic indices could be useful to predict at least the annual worldwide frequency of the largest earthquakes.

The issue is important because although some authors have found correlations between earthquake occurrence and the lunar solid tides on short timescales (e.g., Chen et al. 2012; Cochran et al. 2004; Riguzzi et al. 2010) and solar activity cycles (Choi and Maslov 2010; Choi and Tsunoda 2011; Choi 2013), the long-term triggering effect of the lunar and solar periodicities is less certain. Oscillations at the 9- and 20-year periods were found in some local records such as in southern California and in Japan (e.g., Kilston and Knopoff 1983; Tanaka 2014).

There might be a need to take into account additional effects linked to climatic and oceanic circulation changes to reach critical effects comparable with the earthquake stress drop threshold. In any case, earthquake triggering can occur also when the stress perturbation is only 1/10 of the secular stress accumulation rate (i.e., an order of magnitude of 1 kPa/year), not of the stress drop (order of MPa) (cf., Heki 2003).

This paper aims to establish whether an earthquake–climate worldwide link exists at the decadal and multidecadal scales and to provide an approximated earthquake worldwide annual frequency forecast for the next decades. We analyze the NOAA Significant Earthquake Historical database ¹. This NOAA catalog contains information on destructive earthquakes from 2150 B.C. to the present that meet at least one of the following criteria: moderate damage (approximately \$1 million or more), 10 or more deaths, magnitude 7.5 or greater, modified Mercalli intensity X or greater, or generated a tsunami.

We notice that another worldwide catalog exists: the Centennial Earthquake catalog ². However, herein, we have preferred the NOAA Significant Earthquake Historical database because it could provide a well-defined record. It automatically excludes all $M < 7.5$ earthquakes that do not cause significant damages, which could imply that an earthquake cluster be counted only once in many cases. Moreover, the Significant Earthquake Historical database collects events from the worldwide inhabited regions, which is a well-defined region. These events are certain, and their record could be a better representative of the statistics of the phenomenon, although it represents a subset of all events. On the contrary, the Centennial Earthquake Catalog may be partial and may introduce biases and

¹ <http://www.ngdc.noaa.gov/hazard/earthqk.shtml>.

² <http://earthquake.usgs.gov/data/centennial/>.

inhomogeneities because the catalogs from the uninhabited regions could be underreported and fragmented. A careful analysis of the Centennial Earthquake Catalog is, therefore, left to another dedicated study that should take into account issues about its completeness, homogeneity, and aftershock cluster patterns. Finally, we choose the Significant Earthquake Historical database also because of its higher natural hazard and social-economical importance.

2 $M \geq 7$ earthquake annual frequency data and analysis

The earthquake frequency of the NOAA Significant Earthquake Historical database varies greatly in time. Before 1900, very few earthquakes are reported and only from specific regions such as the latitude range $30^{\circ}\text{N} - 50^{\circ}\text{N}$ and from Central and South America. The annual frequency of the database since 1800 is shown in Fig. 1: red curve for earthquake magnitude $5 \leq M < 6$; green curve for earthquake magnitude $6 \leq M < 7$; and blue curve for earthquake magnitude $M \geq 7$.

Figure 1 suggests that the earthquake occurrence was underreported before 1900. The earthquake frequency with magnitude $M < 7$ gradually increased during the twentieth century. This is likely an artifact due to the incompleteness of the catalog because small earthquakes are orders of magnitude more frequent than the large ones (Gutenberg and

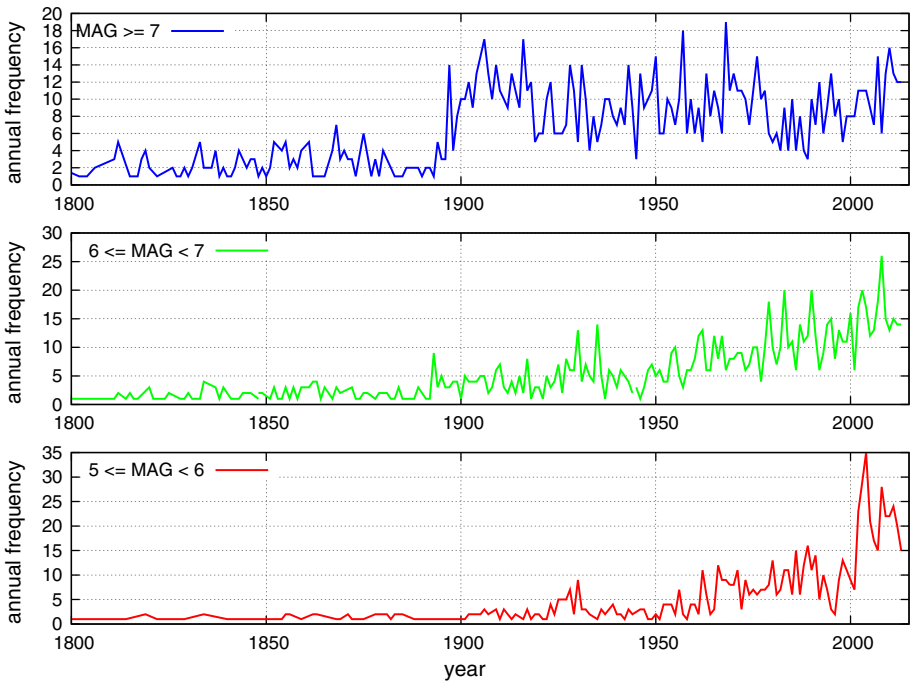


Fig. 1 Annual frequency of the NOAA significant earthquake historical database for earthquake magnitude $5 \leq M < 6$ in red, for earthquake magnitude $6 \leq M < 7$ in green and for earthquake magnitude $M \geq 7$ in blue. Only the post-1900 part of the blue curve seems to be physically relevant because it appears statistically stationary. (Data from <http://www.ngdc.noaa.gov/hazard/earthqk.shtml>)

Richter 1954). Thus, using the $M < 7$ earthquake data introduce artificial bias in the analysis: A fact that needs to be avoided. On the contrary, the annual frequency for the $M \geq 7$ earthquakes (blue curve in Fig. 1) appears to be quite stationary since 1900.

In the following, we assume that the NOAA earthquake catalog for the $M \geq 7$ earthquakes since 1900 is the one relevant for our analysis, and that its patterns represent real dynamical properties. In Appendix 1, we discuss in details the issue regarding the magnitude of completeness according the Gutenberg–Richter relation (cf. Gutenberg and Richter 1954; Mignan and Woessner 2012) and argue that adopting the $M = 7$ threshold can be a reasonable choice.

Figure 1 shows that the $M \geq 7$ earthquake annual frequency sequence is characterized by fast fluctuations plus multidecadal patterns with maxima occurring in the 1910s, in the 1970s, and after 2010, and minima in the 1930s and in the 1980s. Thus, there appears to be a 50- to 60-year oscillation (cf., Mogi 1979; Möner 1989).

Figure 2 shows the worldwide areal and temporal distribution of the $M \geq 7$ earthquakes occurred since 1900 when the distribution of the events is more worldwide indicative. Most worldwide largest earthquakes occurred at the land boundaries of the Pacific Plate, which includes also the Philippine Plate, the Cocos Plate (Pacific cost of Central America and Mexico), and the Mazca Plate (Pacific coast of South America). In fact, all around the Pacific Ocean basin, there are convergent plate boundaries that cause frequent earthquakes and strong volcanic eruptions. Because of the latter, the same zone is also known as the Ring of Fire.

The left panel in Fig. 2 depicts the earthquake frequency for latitude degree. It is observed that very few $M \geq 7$ earthquakes occur close to the polar regions (longitude ranges $90^{\circ}\text{S} - 60^{\circ}\text{S}$ and $60^{\circ}\text{N} - 90^{\circ}\text{N}$) and that most earthquakes occur between latitude 30°S and latitude 50°N . The earthquake distribution appears to be bimodal with peaks of about 14 earthquakes per degree in the latitude ranges $20^{\circ}\text{S} - 0^{\circ}$ and $30^{\circ}\text{N} - 50^{\circ}\text{N}$. This earthquake distribution is skewed toward the Northern Hemisphere likely because this hemisphere has more coastal subduction zones. The general evidence is that there are more earthquakes around the equator and close to latitude 40°N than close to the poles. The area close to latitude 40°S presents few earthquakes likely because there is very little land at that latitude. However, at that latitude, most earthquakes are concentrated in New Zealand.

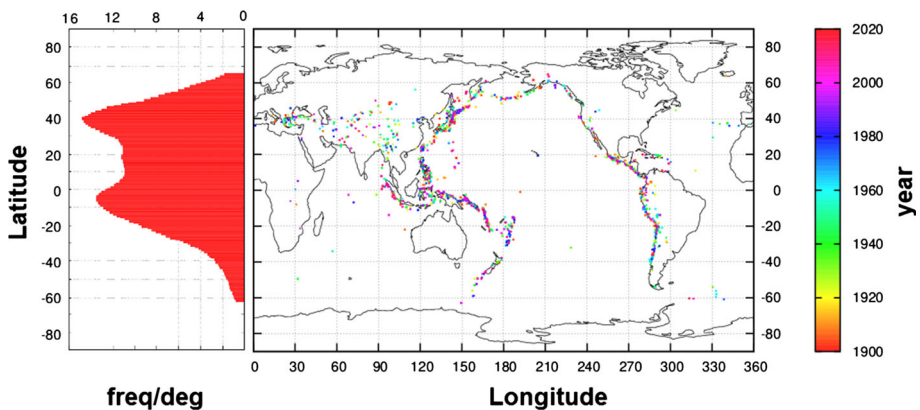


Fig. 2 $M \geq 7$ since 1900. The occurrence date is indicated by the color. The left panel depicts the earthquake frequency for latitude degree

Figure 3 shows a Hurst analysis of the $M \geq 7$ earthquake annual frequency record since 1900. The scaling analysis is based on the standard deviation algorithm (SDA) that evaluates the Hurst exponent H defined from the diffusion function $D(l) \propto l^H$ (Scafetta and Grigolini 2002; Scafetta and West 2004a; Scafetta et al. 2004b; Scafetta 2010a). The time window length l measures the auto-correlation time interval: if the Hurst exponent is $H \approx 0.5$, the sequence is random; if $H > 0.5$, the sequence presents a long-range memory and a positive persistence; if $H < 0.5$, the sequence presents a negative persistence.

Figure 3 shows in blue the SDA function for the original record, which gives $H = 0.64$, and for the same record after temporal shuffling, which gives $H = 0.50$ as expected for random sequences. Thus, the $M \geq 7$ earthquake frequency record since 1900 is not made of events that occur randomly in time: It clearly obeys a certain dynamics.

Figure 3 shows that as the time window length l increases, the blue SDA function $D(l)$ decreases after $l = 30$ years. This is in part due to the fact that as l increases the statistical accuracy of the analysis decreases due to the 114 data points length of the analyzed record. This is implied also by the decay of the red curve for $l > 30$, which shows the SDA for the shuffled record. However, the same blue curve reaches a minimum around $50 < l < 60$ and then it rises again. This specific pattern in the SDA curve could be typically induced by an oscillation with a period of 50–60 years (Scafetta 2010a; Scafetta and West 2004).

Figure 4 shows two alternative power spectrum evaluations of the $M \geq 7$ earthquake frequency sequence since 1900. The power spectra use the maximum entropy method (MEM) and the multi-taper method (MTM) (Ghil et al. 2002). The 95 and 99 % confidence level refers to the MTM method. MTM reveals a major spectral peak (99 % confidence) at

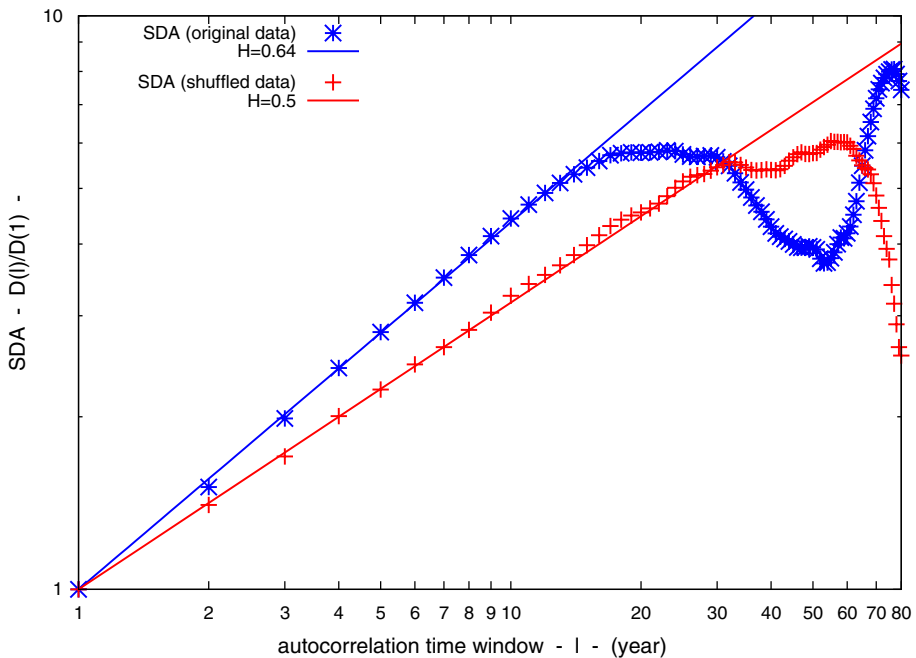


Fig. 3 Hurst-based scaling analysis of the $M \geq 7$ earthquake frequency sequence since 1900. The scaling analysis is based on the standard deviation algorithm (SDA) (Scafetta and Grigolini 2002; Scafetta and West 2004a)

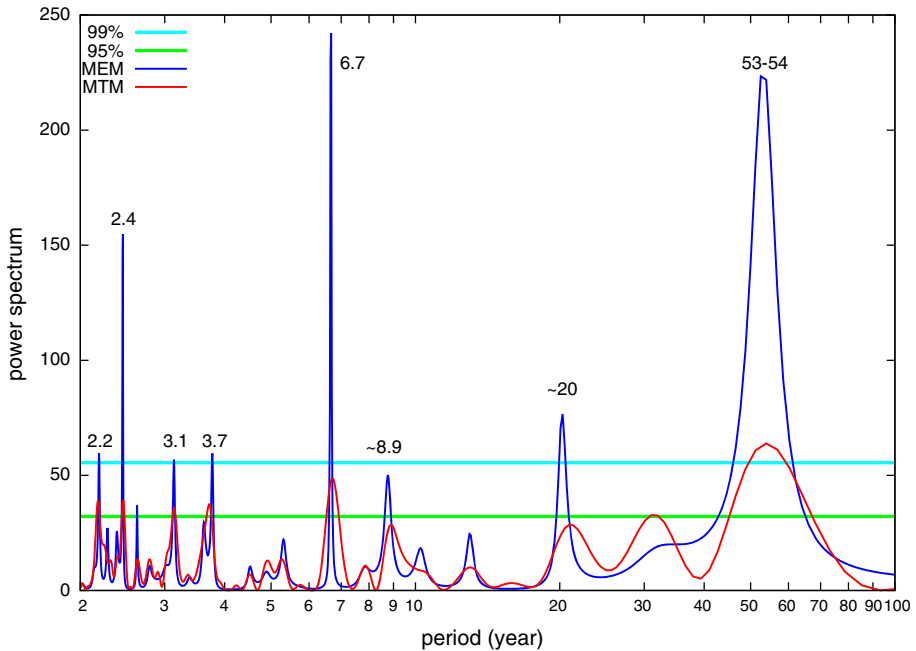


Fig. 4 Power spectrum evaluations of the $M \geq 7$ earthquake sequence since 1900. The power spectra use the maximum entropy method (MEM) and the multi-taper method (MTM) (Ghil et al. 2002)

a period of $p = 54 \pm 12$ years (99 % confidence). The result is confirmed by MEM that also reveals possible harmonics at periods of 2.2, 2.4, 3.1, 3.7 and 6.7 years, and at the periods $p = 8.9 \pm 0.4$ years and $p = 20 \pm 2$ years.

An analysis of possible earthquake repetition/aftershocks at short time and area scales was made. On a total of 1,087 $M \geq 7$ events from 1900 to 2013, we found: 39 events occurred close to other events within 6 months and 0.5° coordinate (about 56 km radius); 47 events within 1 year, and 0.5° coordinate; 77 events within 6 months and 1° coordinate (about 111 km radius); 94 events within 1 year and 1° coordinate. The four $M \geq 7$ earthquake sequences since 1900 detrended of these plausible aftershocks are shown in Appendix 2 and their spectral analyses confirm the power spectrum peaks depicted in Fig. 4.

3 The Pacific Decadal Oscillation (PDO) index

Numerous studies have determined that the climate system is regulated by a large 50- to 70-year oscillation lasting for centuries and millennia in a variety of climatic records such as ice core samples, three ring records, fish catching and sediment records, global surface temperature records, monsoon records, sea level oscillation records, Atlantic Multidecadal Oscillation (AMO), North Atlantic Oscillation Index (NAO), Pacific Decadal Oscillation (PDO), snowfall time series, and many others (e.g., Davis and Bohling 2001; Enzi et al. 2014; Klyashtorin and Lyubushin 2007; Klyashtorin et al. 2009; Knudsen et al. 2011; Jevrejeva et al. 2008; Loehle and Scafetta 2011; Mazzarella 2013; Mazzarella and Scafetta

2012; Qian and Lu 2010; Scafetta 2010a; Scafetta et al. 2013; Wyatt and Curry 2013, and many others). Also quasi 9- and 20-year oscillations have been observed in the climate system (e.g., Chylek et al. 2011; Manzi et al. 2012; Scafetta 2010b, 2013b, 2014c).

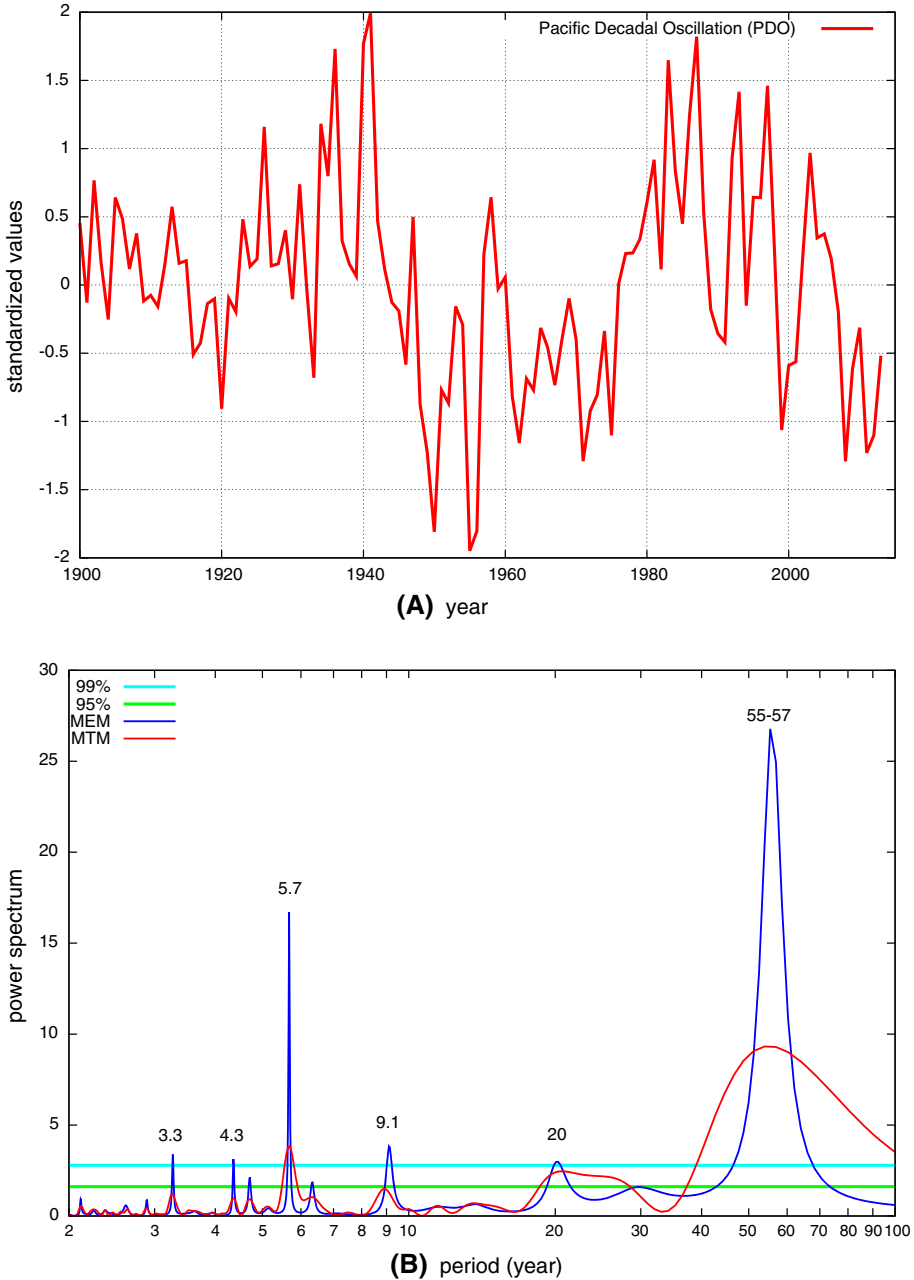


Fig. 5 [A] Pacific Decadal Oscillation (PDO) index. [B] Its power spectrum evaluations using MTM and MEM. (Data from <http://jisao.washington.edu/pdo/>)

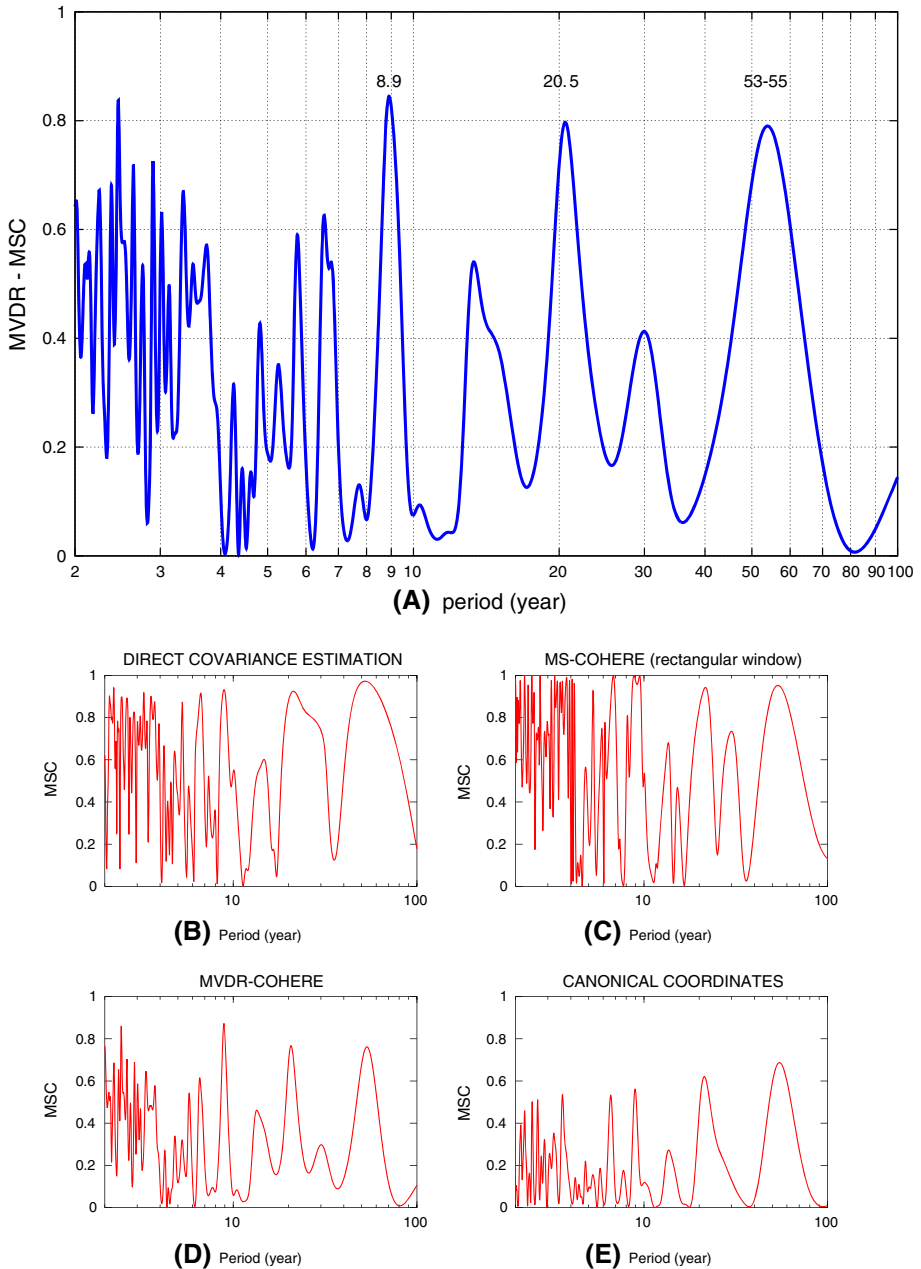


Fig. 6 Magnitude squared coherence (MSC) analysis between the PDO index and the $M \geq 7$ earthquake annual frequency record using: **a** the *minimum variance distortion-less response* (MVDR) method with windows of $M = 87$ years ($3/4$ of the 114-year available record); **b** the direct covariance matrix estimation; **c** the MATLAB MS-Cohere algorithm using the rectangular window; **d** the MVDR-cohere method; **e** the canonical coordinate analysis. The **b, c, d, e** panels use windows of $M = 76$ years ($2/3$ of the 114-year available record). The MSC algorithms are from Welch (1967); Carter et al. (1973); Benesty et al. (2006); Santamaria and Via (2007). Note the three common coherence peaks at periods of about 9, 20 and 50–60 years

Figure 5A shows the Pacific Decadal Oscillation (PDO) index that is a long-lived El Niño-like pattern of the Pacific climate variability. The PDO record is herein chosen because most of the NOAA significant earthquake historical events occurred at the land boundaries of the Pacific Plate (Fig. 2). The JISAO Web site describes the PDO variability as: “Cool PDO regimes prevailed from 1890–1924 and again from 1947–1976, while warm PDO regimes dominated from 1925–1946 and from 1977 through (at least) the mid-1990’s. Shoshiro Minobe has shown that twentieth century PDO fluctuations were most energetic in two general periodicities, one from 15-to-25 years, and the other from 50-to-70 years” (from <http://jisao.washington.edu/pdo/>).

Figure 5B shows the power spectrum evaluation of the PDO index. A major spectral peak is found at the period $p = 56 \pm 14$ years, and minor spectral peaks at periods of $p = 9.1 \pm 0.4$ years and $p = 20 \pm 2$ years. These periods are statistically coherent with those found in several global surface and ocean temperature records (Scafetta 2010a, 2014a) and in the earthquake record (Fig. 4).

4 Magnitude squared coherence analysis

A spectral coherence between the PDO index and the $M \geq 7$ earthquake sequence at the 9-, 20-, and 50- to 60-year periods is confirmed by the magnitude squared coherence (MSC) analysis: see Fig. 6. We use four standard magnitude square coherence methodologies (Benesty et al. 2006; Carter et al. 1973; Santamaria and Via 2007; Welch 1967): the direct covariance matrix estimation; the MATLAB MS-Coher algorithm using the rectangular window; the minimum variance distortion-less response (MVDR) method; the canonical coordinate analysis.

The MSC index approaches 1 when two sequences are characterized by a common frequency despite the size of their mutual amplitude. Figure 6 shows $MSC \gtrsim 0.7$ for at least three common periods at $p_9 = 8.9 \pm 0.5$ years, $p_{20} = 20.5 \pm 2.4$ years and $p_{60} = 54 \pm 17$ years.

The earthquake and the PDO records also show significant spectral peaks at $p = 6.7 \pm 0.2$ years and $p = 5.7 \pm 0.2$ years, respectively. Whether this 1-year period difference is an artifact of some high-frequency data imprecision in one or both records cannot be determined from this analysis. Below a direct comparison between the two records will be limited to the decadal and multidecadal scales.

The spectral coherence found between the $M \geq 7$ earthquake annual frequency record and the PDO index can be extended to numerous other climatic indexes because the latter are coherent to each other as explained in Sect. 3. Thus, we conclude that there exists a relationship between the $M \geq 7$ earthquake annual frequency record and the climate indexes.

5 A tentative harmonic forecast

The physical origin of the quasi 9-, 20-, and 50- to 70-year oscillations is likely astronomical given the fact that similar oscillations are found among the decadal and multidecadal lunar and solar oscillations (Scafetta 2010b, 2012b, 2013b, 2014b, c).

Among the lunar decadal and multidecadal cycles, there are the 8.85-year apside precession cycle, the 18.03-year Saros eclipse cycle with its 9.01-year second harmonic, the

18.61-year lunar nodal and inclination cycle with its 9.3-year second harmonic, and the 54.093-year triple Saros cycle, that is, when the Sun, Earth, and Moon return to approximately the same relative geometry and a nearly identical eclipse occurs at the same location on Earth. Solar and heliospheric oscillations are observed at periods of about 20 years (synodic cycle of Jupiter and Saturn, major oscillation in the solar wobbling, aurora records), 22 years (Hale solar magnetic cycle) and 60 years (aurora, solar and heliospheric oscillation) (Ogurtsov et al. 2002; Scafetta 2010a, 2012a, b, c; Scafetta and Willson 2013).

If the $M \geq 7$ earthquake frequency sequence is modulated by astronomical oscillations, it is possible to provide an approximate harmonic forecast. Figure 7 shows the earthquake record fit with a 54-year oscillation under the hypothesis that this oscillation is regulated by the triple Saros solar–lunar tidal cycle, and by a 60-year oscillation under the hypothesis that is driven by solar–heliospheric harmonics. We found the following regression equations using the three decadal and multidecadal harmonics:

$$f_{54}(t) = 1.84 \sin[2\pi(t/54 + 0.940)] + 0.89 \sin[2\pi(t/20 + 0.698)] + 0.95 \sin[2\pi(t/9 + 0.690)] + 9.41 \quad (1)$$

$$f_{60}(t) = 1.72 \sin[2\pi(t/60 + 0.568)] + 0.94 \sin[2\pi(t/20 + 0.701)] + 0.96 \sin[2\pi(t/9 + 0.689)] + 9.57 \quad (2)$$

The standard deviation residual of the fitting is almost the same: 2.95 earthquake/year using Eq. 1 and 3.00 earthquake/year using Eq. 2.

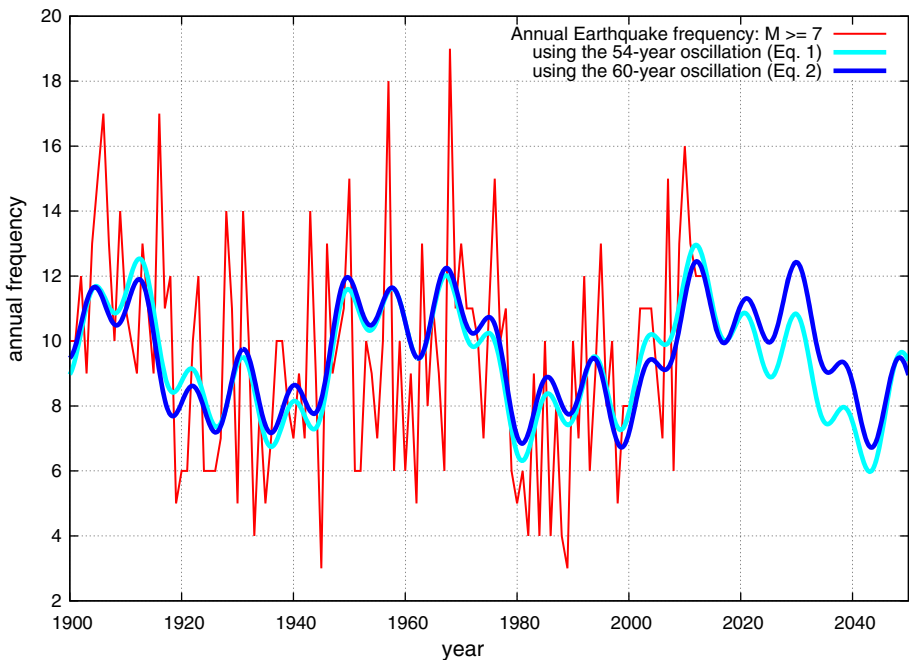


Fig. 7 $M \geq 7$ earthquake annual frequency sequence fit with two regression functions with 54-year and 60-year periods, plus the 20- and the 9-year cycles (Eq. 1 and 2)

The two sinusoidal fits depicted in Fig. 7 suggest that the next 15 years will be characterized by a relatively high earthquake activity with on average 10–12 large $M \geq 7$ events per year.

A simple comparison between the PDO index of Fig. 5a and the $M \geq 7$ earthquake annual frequency sequence of Fig. 7 shows that their multidecadal 50- to 60-year oscillations are negatively correlated. Therefore, at this timescale, there are more $M \geq 7$ earthquakes during the cool PDO phase (that is, when the American West coast cools and the Asian–Australian East coast warms), and less $M \geq 7$ earthquakes during the warm PDO phase (that is, when the American West coast warms and the Asian–Australian East coast cools) (cf., Choi and Maslov 2010).

To study how the cross-correlation phase evolves in function of the timescale, the PDO index is first fit using the following regression equation:

$$f_{PDO}(t) = 0.50 \sin[2\pi(t/56 + 0.746)] + 0.27 \sin[2\pi(t/20 + 0.151)] + 0.24 \sin[2\pi(t/9.1 + 0.966)] + 0.01 \tag{3}$$

Figure 8 compares the correspondent three harmonic constituents between the PDO index (Eq. 3, red curves) and the $M \geq 7$ earthquake annual frequency sequence (we use Eq. 1, blue curves), and their respective residual functions at the sub-decadal scales. Figure 8 shows that at the 50- to 60- and 20-year timescales, the two records are negatively correlated, while at the 9-year timescale, the two records are positively correlated with a

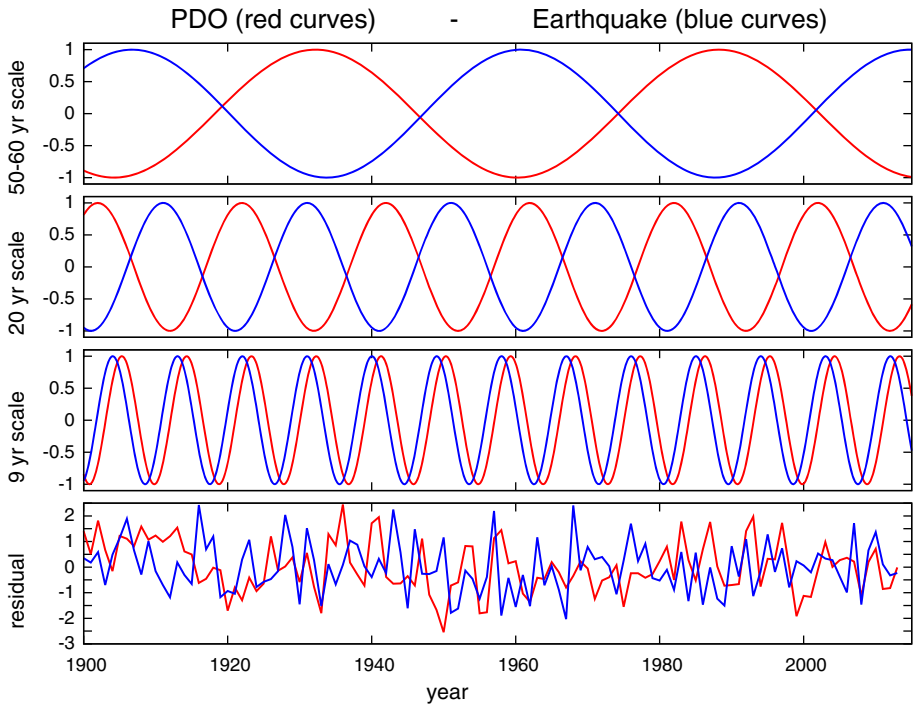


Fig. 8 Visual cross-correlation between the three harmonic constituents at the 9-, 20-, and 50- to 60-year timescales between the PDO index (Eq. 3, red curves) and the $M \geq 7$ earthquake annual frequency sequence (Eq. 1, blue curves), and between their respective residual functions at the sub-decadal scales

possible small 1-year time lag. However, the small time lag may be also due to some imprecision in the records. The correlation between the two residual functions is less certain, although the correlation coefficient is slightly positive, $r = 0.11$ for 114 points, which implies a positive correlation with a probability $P > 75\%$.

6 A possible indirect physical link with the length of the day (LOD) index

Earth does not spin at a stable rate because different processes (tides, atmosphere-ocean circulations, internal phenomena, etc.) are responsible for anomalies from its rotational-hydrostatic equilibrium. The length of the day (LOD) measures changes in the Earth's rotation (Stephenson and Morrison 1995). This index reveals profound effects both on the interior of the planet and on its crust, oceans, and atmosphere owing to the continuous struggle between variable angular momentum and gravitational force (cf., Mörner 2013, fig. 9).

If a link between LOD and earthquake exists, the effect should be enhanced in the equatorial regions relative to the polar ones. Indeed, in Fig. 2, we have verified the latitude dependence of the worldwide number of the $M \geq 7$ earthquakes. The incremental distribution of seismic events shows that polar regions are rarely affected by seismic activity and that most of the events fall in the range $60^\circ\text{S} < \text{lat} < 60^\circ\text{N}$.

Recently, Wang et al. (2000) compared LOD data and earthquake catalogs in China and found interesting correlations between the two indexes. The correlation appeared most typically on the decadal timescales and seemed to be direction dependent. They also

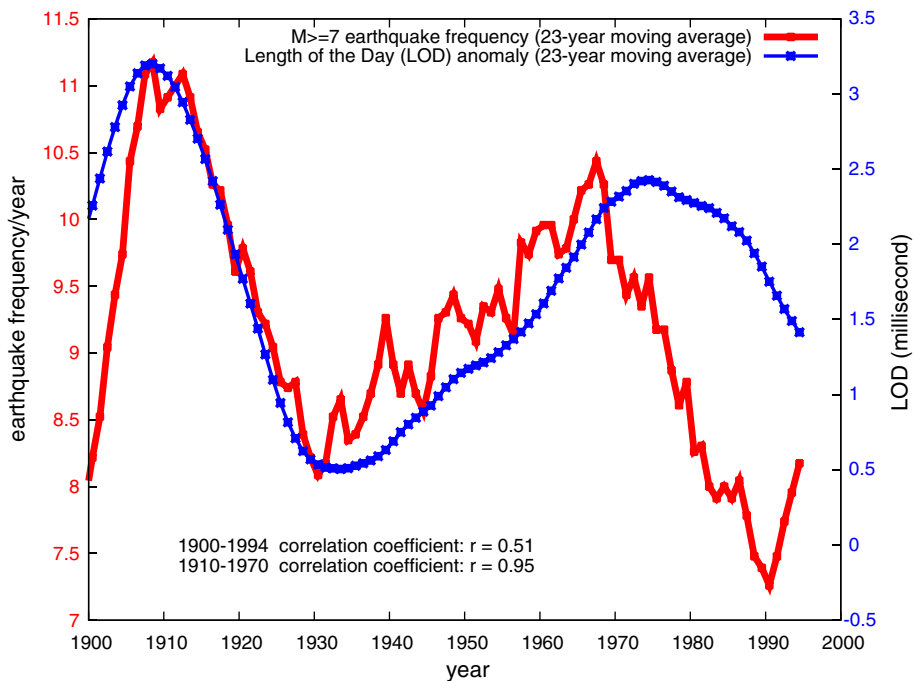


Fig. 9 The $M \geq 7$ earthquake annual frequency sequence against the length of the day (LOD) index. The two indexes are correlated with a probability $P > 99.95\%$

speculated that similar correlation phenomena should exist in other parts of the world although they did not expect that the decade LOD-deformation correlation had always to appear on all monitoring sites or stations. Ostřihanský (2012) found correlation of earthquakes with biweekly tides expressed as LOD variations and suggested that a majority of earthquakes could be triggered in both Earth’s rotation deceleration and acceleration. Ostřihanský (2012) also speculated the existence of longer cycles by observing that the “Great Sumatra earthquake 26 December 2004 had its equivalent in the shape of LOD graph, full Moon position, and character of aftershocks 19 years earlier in difference only one day to 27 December 1985 earthquake, proving that not only sidereal 13.66 days variations but also that the 19 years Metons cycle is the period of the earthquakes occurrence.”

Indeed, Fig. 9 shows the $M \geq 7$ earthquake annual frequency sequence against the LOD. Both records were smoothed with a 23-year moving average algorithm to highlight better the 60-year oscillation. The correlation between the two records is very high: The correlation coefficient is $r = 0.51$ for the period 1900–1994, and is $r = 0.95$ for the period 1910–1970. The good positive correlation between the two records depicted in Fig. 9 suggests that when LOD increases, that is, the angular velocity of the Earth decreases and the compression of the equatorial masses increases, more earthquakes occur, and vice versa.

However, Wang et al. (2000) argued that LOD variations appear to be too small to have some significant effect. For example, the vertical displacement ∇U caused by LOD variation is given by the following equation (cf., Gipson and Ma 1998):

$$\nabla U_{LOD} = -hm_z \frac{\Omega^2 r^2}{g} \sin^2 \theta, \tag{4}$$

where $\Omega = 7.3 \times 10^{-5} \text{ s}^{-1}$ is the average angular velocity of the Earth, θ is the colatitude (it varies from 0° for the north pole to 180° for the south pole), $r = 6.371 \times 10^6 \text{ m}$ is the radius from the center of the Earth, $g = 9.81 \text{ m/s}^2$ is the gravitational acceleration at the Earth’s surface, m_z is the excess length of day (LOD), $h \approx 0.60$ is the vertical Love number. Using Eq. 4, on the equator ($\theta = 90^\circ$) where the effect is the greatest, the vertical displacement is just $\nabla U_{LOD} = -0.45 \text{ mm}$ if $m_z = 3 \text{ ms/day} = 3.5 \times 10^{-8}$, and $\nabla U_{LOD} = -0.08 \text{ mm}$ if $m_z = 0.5 \text{ ms/day} = 5.8 \times 10^{-9}$. Thus, the maximum theoretical vertical displacement change at the equator observed since 1900 is just 0.37 mm. It is unclear whether these little changes may be the first cause that can trigger earthquakes. Gipson and Ma (1998) noted that the LOD-induced vertical displacement is significantly smaller than the pole tides and for most applications could be ignored.

Given the small LOD effect theoretically deduced from Eq. 4, Wang et al. (2000) inferred that the correlated decade variations in LOD, crustal deformation, and stress all originate from the same source, and conjectured a core–mantle coupling process occurring deep in the Earth. However, they also acknowledged that the theoretical models describing how the crust or lithosphere respond to the core–mantle coupling are still missing.

The lack of theoretical understanding may imply alternative explanations. For example, there might be a significant climatic/oceanic triggering effect through various mechanisms, as suggested by the coherence between the $M \geq 7$ earthquake annual frequency sequence and climatic indexes established in the previous sections. The LOD changes are found correlated with the earthquake record because LOD is modulated by climatic changes as the LOD responses to intense ENSO events and to global surface temperature changes seem to suggest (cf: Mörner 1989; Mazzarella and Scafetta 2012; Mazzarella et al. 2013).

7 Discussion and conclusions

The earthquakes annual frequency sequence of the NOAA Significant Earthquake Historical database collects the information about the earthquakes that have been the most destructive for human societies around the world. The database is likely incomplete before 1900. Only the subset of the $M \geq 7$ earthquake appears stationary since 1900. Most of these events occurred at the land boundaries of the Pacific Plate.

We have found that the annual frequency of the $M \geq 7$ earthquake record is quite stationary, but not random. The $M \geq 7$ earthquake frequency sequence since 1900 is characterized by a persistent long-range memory dynamics that is likely regulated by a large quasi 50- to 60-year oscillation plus additional minor oscillations at periods of about 2.2, 2.4, 3.1, 3.7, 6.7, 9, and 20 years.

The 9-, 20-, and 50- to 60-year periods are found among numerous climatic records (e.g., Chylek et al. 2011; Davis and Bohling 2001; Enzi et al. 2014; Klyashtorin and Lyubushin 2007; Klyashtorin et al. 2009; Knudsen et al. 2011; Jevrejeva et al. 2008; Loehle and Scafetta 2011; Mazzarella 2013; Mazzarella and Scafetta 2012; Manzi et al. 2012; Qian and Lu 2010; Scafetta 2010a; Scafetta et al. 2013; Wyatt and Curry 2013, and many others). This result indicates that the $M \geq 7$ earthquake system may be reasonably linked to climate variability made of changes of temperature, rain, snow, wind, pressure, and ocean currents. In particular, we found a negative correlation between the $M \geq 7$ earthquake frequency record and the PDO index at the 20- and 50- to 60-year timescales, while the correlation is positive at the 9-year and below timescales (Fig. 8). Tanaka (2014) and Ide and Tanaka (2014) also found an approximately 9- and 18.6-year period variation in seismicity, crustal deformation, and tremors in Japan; these authors proposed possible mechanisms based on lunar forcing.

Thus, a physical link between the $M \geq 7$ earthquake record and climate variability exists, but it is timescale dependent. Very likely at least two alternative physical mechanisms regulate the sub-decadal and multidecadal scales. The dynamical property of the coupling is important because it permits to use climatic indexes as predictors of $M \geq 7$ earthquake frequency occurrence.

Also a direct comparison with the LOD highlights a strong positive correlation with the $M \geq 7$ earthquake frequency record: see Fig. 9. However, theoretical estimates of the LOD variation effect on the crust would suggest that the LOD variations could not be the first cause of earthquake occurrence. On the contrary, both phenomena seem to originate from another source, which we conjecture to be climatic and oceanic harmonic changes driven by astronomical forces (e.g., Mörner 2013; Scafetta 2010a, 2013b, 2014c).

We conjecture that solar/lunar/astronomical cyclical forcings cause atmospheric and oceanic circulation changes (Scafetta 2012a, b, 2013b). These changes should induce a variable torque that slightly moves the ocean and stress Earth's crust relative to the mantle. A climatic circulation torque should also cause LOD changes. A LOD feedback can also activate additional climatic changes, for example, linked to changes in the ocean thermodynamics due to the water displacement from the poles to the equator and vice versa. Lunar and solar tidal forcing contributes and facilitates the process by gradually moving the oceans and stressing the crust.

Mazzarella and Scafetta (2012) and Mazzarella (2013) have shown that the integrated NAO yearly values (INAO) is an excellent proxy for atmospheric circulation: Positive values of INAO indicate zonal circulations (along latitude) while negative values of INAO indicate meridional circulations (along longitude). At the multidecadal scale, INAO and LOD are inversely related to each other so that periods of increasing zonal circulation are

accompanied by periods of planet increasing rotational rate, while periods of decreasing zonal circulation speed are accompanied by periods of Planet decreasing rotational rate. Strong zonal circulations cause the contraction of the circumpolar vortex and an increase in Earth rotation, while weak zonal circulations or, equivalently, strong meridional circulations with meandering or cellular patterns cause an expansion of the circumpolar vortex and a decrease in Earth rotation. Scafetta (2014a) found similar oscillations in the sea level, AMO, PDO, and NAO indexes. Oscillations in the atmospheric and oceanic circulation exercise a variable torque acting on the Earth's crust that causes the LOD oscillations and, therefore, may also facilitate earthquake occurrence.

A link between earthquakes and climatic indexes have been suggested in the case of snow and glacier load changes (e.g., Heki 2003; Pagli and Sigmundsson 2008; Wu and Johnston 2000), typhoons and rain (e.g., Liu et al. 2009; Miller 2008; Saar and Manga 2003), ocean loading that can also vary because of sea level changes (e.g., Luttrell and Sandwell 2010). Also associations with the changes in LOD and ENSO events have been observed (e.g., Mörner 1989, 1998, 2013; Ostrihanský 2012; Riguzzi et al. 2010; Wang et al. 2000). Ohtake and Nakahara (1999) found a significant seasonality in the occurrence time of past great earthquakes ($M \geq 7.9$) in the northwestern margin of the Philippine Sea plate concluding that a small stress increase may trigger an earthquake when the future focal zone is at a critical condition to release a large rupture, but their testing of a possibility of stress change caused by annual variation of the atmospheric pressure was unsatisfactory.

In general, several evidences suggest that a changing climate may trigger earthquakes, tsunamis, and volcanoes (McGuire 2013) although the mechanisms remain unclear. However, all physical mechanisms that could explain how climate phenomena can trigger earthquake proposed in the referenced literature are tentative. Although each individual earthquake may be mostly triggered by a specific climate-related mechanism, on a global scale, numerous climatic indexes are synchronized to each other (e.g., Mazzarella and Scafetta 2012; Scafetta 2010a, 2014a; Wyatt and Curry 2013). This explains why on a global scale, the common climate harmonics appear in the worldwide earthquake index too, and the latter well correlates also with the LOD, which should integrate all climate circulation phenomena.

Riguzzi et al. (2010) noted that “the oscillating horizontal component of the tides load and pump the tectonic system, drop by drop, slowly but steadily, whereas the vertical component of the tides might be the unloading mechanism when enough energy has accumulated along fault zones.” Riguzzi et al. (2010) also noted that “the Gutenberg–Richter law supports that the whole lithosphere is a self-organized system in critical state, i.e., a force is acting contemporaneously on all the plates and distributes the energy over the whole lithospheric shell, a condition that can be satisfied by a force acting at the astronomical scale.”

The found 9, 20, and 50–60 year harmonics are typical lunar, solar, and heliospheric harmonics that were speculated to trigger climate changes (e.g., Scafetta 2010a, 2013b, 2014b, c). Under this hypothesis and because astronomical harmonics can be forecast, approximate worldwide $M \geq 7$ earthquake annual frequency forecast at least at the decadal and multidecadal scales are possible. The harmonic forecast depicted in Fig. 7 suggests that the next 15 years could be characterized by a relatively high earthquake activity with on average 10–12 large $M \geq 7$ events per year. Because $M < 7$ earthquakes are usually aftershocks of the most energetic ones, the worldwide earthquake activity will stay high during the next 15 years with possible maxima in 2020 and 2030 and a minimum in the 2040s, as shown in Fig. 7.

In conclusion, our results indicate that NOAA Significant Earthquake Historical $M \geq 7$ earthquake annual frequency record shows a significant coherence with climatic records at multiple frequencies and a strong correlation with the LOD at the multidecadal scale. A drawback in the analysis may be seen in the fact that only data since 1900 could be analyzed and the record may be too short to well identify a quasi 50- to 60-year oscillation. However, it may be unlikely that the results herein depicted, which involve also oscillations at about 9- and 20-year periods, are just coincidences. Because the observed oscillations are coherent to known astronomical harmonics (Scafetta 2010b, 2012b, 2013b, 2014c) we conclude that understanding how lunar, solar, and possible other astronomical forcings can act on the Earth's geophysics is crucial to advance this field of research. Indeed, since antiquity Babylonians and others have deemed the existence of a possible astronomical influence on climate change and on numerous natural hazards such as earthquake, flood and famine (Pliny the Elder, A.D. 77–79; Forbes 1966) but, even if so, the physical mechanisms are still poorly understood.

Although other earthquake records collected using different criteria may not show identical patterns (see Appendix 1), the results that we found may simply suggest that the NOAA Significant Earthquake Historical $M \geq 7$ earthquake annual frequency record is the most appropriate index to reveal a link between earthquakes and climatic records on a global scale. One reason might also be that the inhabited regions are more sensitive to climatic changes because usually close to the ocean as Fig. 2 shows, and/or to other water supplies. There may be two reasons why the correlation with smaller earthquakes is harder to be seen: (1) Declustering is not working properly for smaller earthquakes and (2) the physical cause of the 9-year periodicity gives larger effects on large earthquakes. As for (2), if a spatial scale of the stress perturbation is larger, larger earthquakes are more likely to be triggered.

Acknowledgments The authors thank the two anonymous referees and Giuliano F. Panza for useful suggestions.

Appendix 1: The threshold of the magnitude of completeness

In the main paper, we have studied the NOAA Significant Earthquake Historical $M \geq 7$ earthquake annual frequency record under the assumption that since 1900 this record is statistically stationary, as shown by the top panel in Fig. 1. Assessing the magnitude of completeness of earthquake catalogs is necessary for any seismic analysis and for avoiding mistakes due to pattern artifacts caused by data incompleteness. However, there is no unique methodology to handle this issue and any statistical strategy may be unsatisfactory for some reason.

The earthquake completeness issue is usually addressed by assuming the validity of the Gutenberg–Richter relation predicting that earthquakes in any given region and time period are distributed in function of their magnitude (Gutenberg and Richter 1954) according to the equation

$$\log_{10}(N) = a - bM \quad (5)$$

where on average $b \approx 1$: however, b can vary between 0.5 and 1.5 depending on the specific tectonic environment of the region (Bhattacharya et al. 2009). Gutenberg–Richter analysis of several earthquake catalogs has shown that the relation should be fulfilled for

local catalogs and $M \leq 7$ (cf. Mignan and Woessner 2012), while for $M \geq 7$ statistical fluctuations and statistical deficiency may characterize the distributions.

Figure 10 shows the magnitude frequency curve of the NOAA Significant Earthquake Historical catalog. It is evident that for $M < 7$ the catalog is severely incomplete because the trend does not fit the Gutenberg–Richter relation. There are also about 300 earthquakes with no reported magnitude. However, a question rises whether the threshold of the magnitude of completeness should be chosen to be $M = 7$, as chosen in the paper, or 7.5 as Fig. 10 suggests given the fact that there are more events in the $7.5 \leq M < 8$ bin than in the $7 \leq M < 7.5$ bin.

The NOAA Significant Earthquake Historical database uses the $M \geq 7.5$ threshold as one of its sufficient although not necessary collection criteria (<http://www.ngdc.noaa.gov/hazard/earthqk.shtml>). Thus, the catalog is very likely complete for $M \geq 7.5$. However, in statistical analysis, it is also important to avoid under-sampling and to reduce non-stationarities due to stochastic fluctuations by using as many data as possible. Discarding the $7 \leq M < 7.5$ data would mean to use 665 instead of 1,087 data, which could significantly reduce the statistical reliability of the record.

In Fig. 10, the tail of the distribution is fit with two alternative Gutenberg–Richter functions, Eq. 5. The blue fit curve produces the Gutenberg–Richter coefficient $b \approx 1$, that is, the expected value considering that the catalog collects worldwide events. The blue fit curve suggests that $M = 7$ could be the optimal value for the magnitude of completeness threshold because it is consistent with the Gutenberg–Richter trend observed for the $M \geq 8.5$ earthquakes and with the local earthquake catalogs that are characterized by a

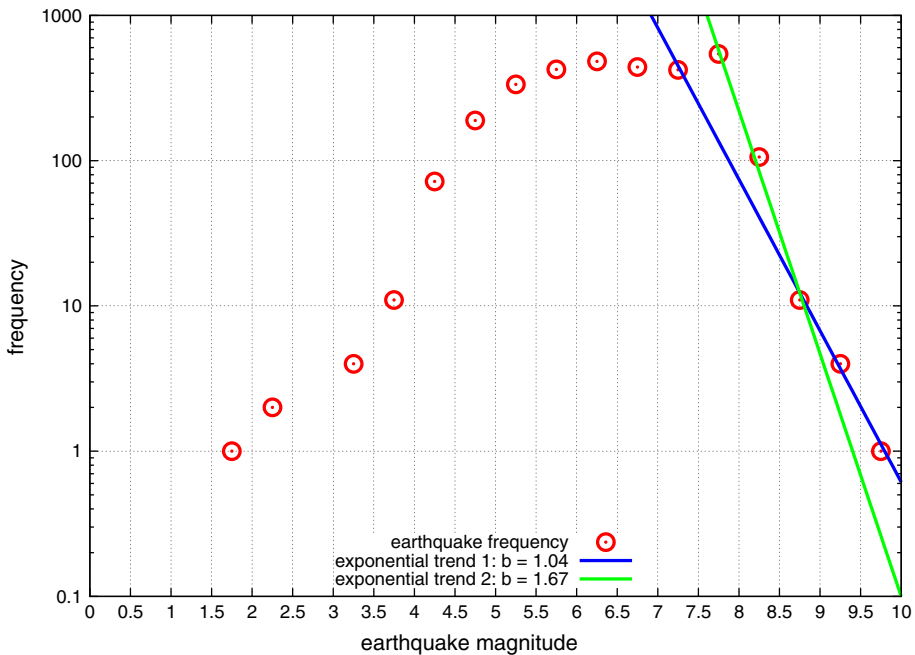


Fig. 10 The magnitude frequency histogram curve of the post-1900 NOAA Significant Earthquake Historical catalog using bin width of $\nabla M = 0.5$. The tail is fit with two alternative Gutenberg–Richter functions, Eq. 5. The blue curve reproduces the expected Gutenberg–Richter coefficient $b \approx 1$

Gutenberg–Richter average exponent $b \approx 1$ for $M < 7$ (cf. Bhattacharya et al. 2009; Gutenberg and Richter 1954; Mignan and Woessner 2012). Moreover, as shown in Fig. 1 the $M \geq 7$ earthquake annual frequency sequence is quite stationary since 1900.

On the contrary, the green curve depicted in Fig. 10 predicts a Gutenberg–Richter exponent of $b \approx 1.67$. While the green curve well fits the three dot regions for $7.5 \leq M < 9$, $b \approx 1.67$ does not seem compatible with Gutenberg–Richter law, which predicts an average exponent $b \approx 1$. Thus, the frequency peak observed in Fig. 10 in the $7.5 \leq M < 8$ bin appears to be a non-stationary statistical fluctuation of the data or an end-of-distribution tail pattern where the Gutenberg–Richter law is not valid any more.

The non-stationarity of the $M \geq 7.5$ earthquake annual frequency sequence is confirmed in Fig. 11: From 1900 to 1920, there are 9.3 ± 0.7 events per year, while from 1920 to 2014, there are 5 ± 0.2 events per year. However, even if quite disrupted by its non-stationarity, a quasi 50- to 60-year oscillation is still visible (maxima around 1910, 1965, 2020 and minima around 1940 and 1980–1990). Thus, the coherence between the earthquake catalog and the climatic indexes at the 50- to 60-year scale appears confirmed also by the restricted $M \geq 7.5$ earthquake annual frequency sequence. For the above reasons, in the paper, we have assumed that the $M \geq 7$ earthquake annual frequency sequence is the most significant one for our analysis.

As explained in the Introduction, the Centennial Earthquake catalog contains more events than the NOAA Significant Earthquake Historical database. The latter was preferred here because the former may also add a number of aftershocks that need to be filtered off for our analysis and, in any case, the latter is made of events occurred in the worldwide inhabited regions, which are certain, while the data from the uninhabited regions may be more fragmented. Our comparison between the two records suggests that they are almost

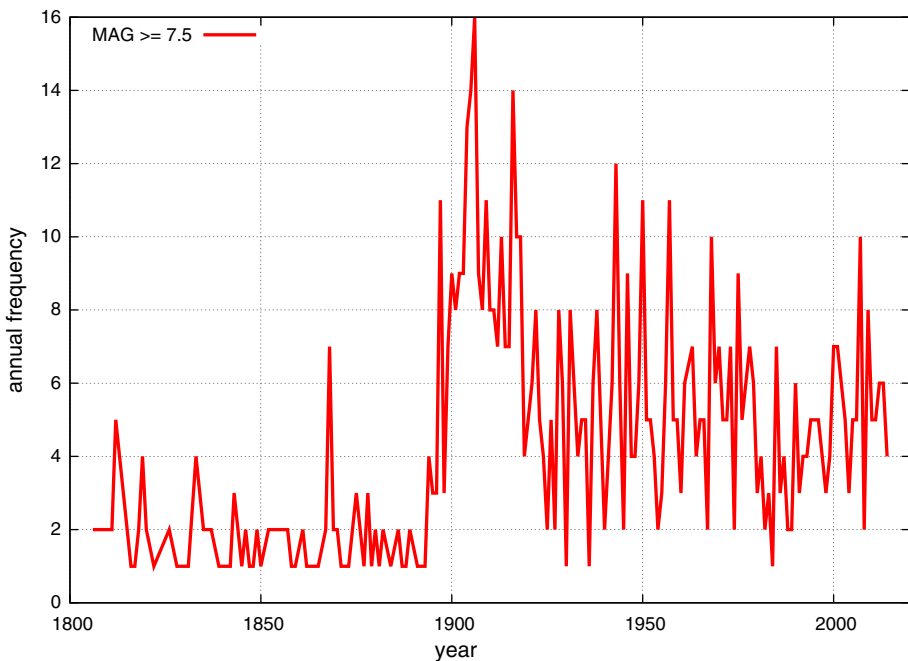


Fig. 11 The $M \geq 7.5$ earthquake annual frequency sequence

equivalent for the $M \geq 7.5$ earthquakes: The Centennial Earthquake catalog lists 422 events against 665 events of the NOAA Significant Earthquake Historical database. For the $7 \leq M < 7.5$ earthquakes, the Centennial Earthquake Catalog contains a number of events

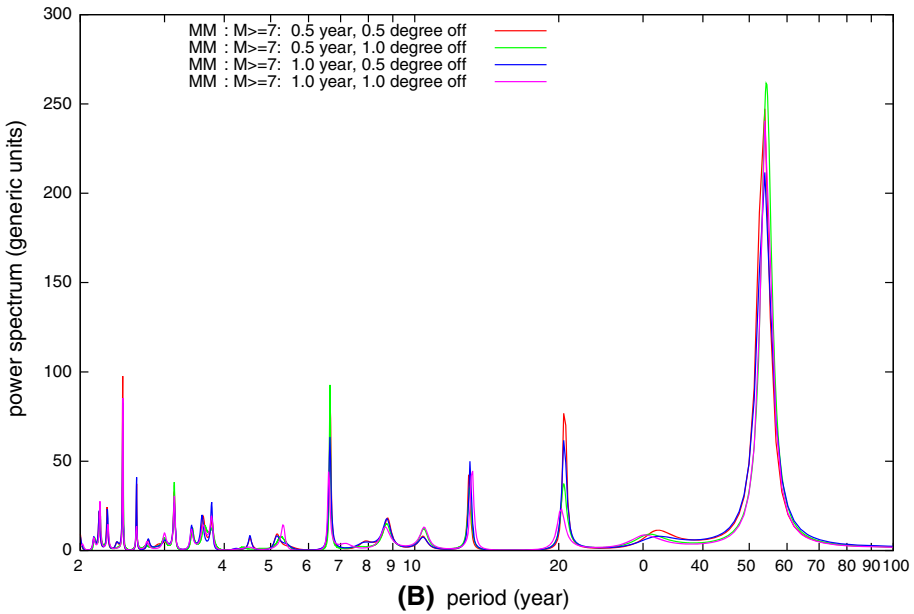
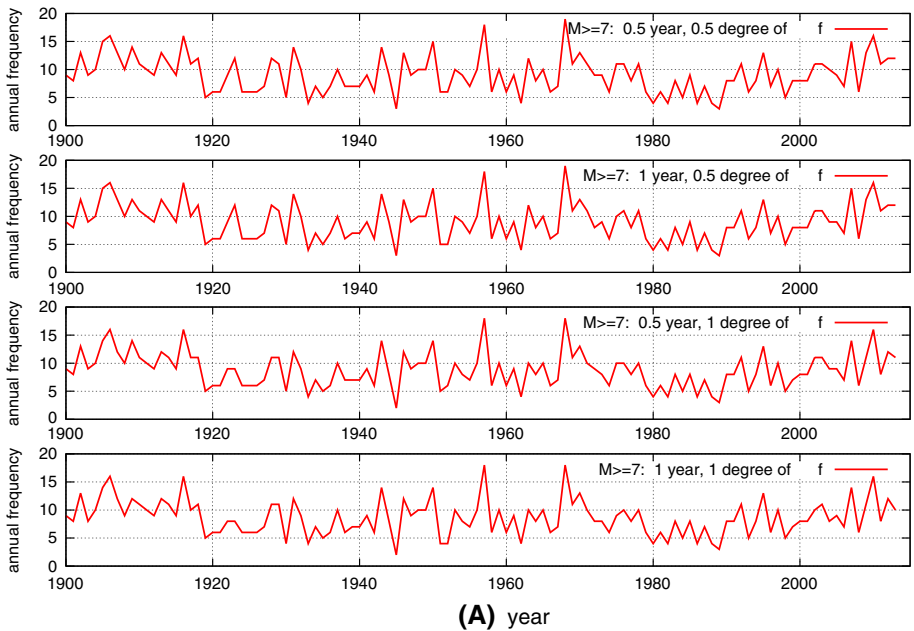


Fig. 12 **a** Four $M \geq 7$ earthquake sequences since 1900 detrended of plausible aftershocks at short time and area scales. **b** Their MEM spectral analysis

that is almost 3 time larger than the NOAA catalog: 1235 versus 422. The $M \geq 7$ Centennial Earthquake annual frequency sequence approximately mirrors a similar non-stationarity as seen in Fig. 11 presenting an average of 17 events per year for the period 1900–1950 and about 14 events per year for 1950–2007. Thus, it is possible that many of the reported $7 \leq M < 7.5$ earthquakes are aftershocks of the $M \geq 7.5$ earthquakes that have not been reported in the NOAA catalog because they did not cause significant damages, while the NOAA catalog may reports more independent events. In any case, the $M \geq 7$ Centennial Earthquake annual frequency sequence presents harmonic patterns disrupted relative to the NOAA $M \geq 7$ earthquake annual frequency record shown in Fig. 1. Understanding this difference requires a dedicated study.

Appendix 2: Removing aftershocks at short time and area scales

Seismicity declustering is the process of separating an earthquake catalog into foreshocks, mainshocks, and aftershocks. Declustering is widely used in seismology, in particular, for seismic hazard assessment and in earthquake prediction models and several advanced algorithms have been proposed (Knopoff 1964; Stiphout et al. 2012). Here, we adopt a simpler strategy to verify that the NOAA Significant Earthquake Historical earthquake catalog herein studied is sufficiently declustered and that the spectral results are sufficiently robust under data declustering corrections.

Figure 12A shows four $M \geq 7$ earthquake sequences since 1900 detrended of plausible aftershocks. On a total of 1,087 $M \geq 7$ events from 1900 to 2013, we found: 39 events occurred close to other events within 6 months and 0.5° coordinate (about 56 km radius); 47 events within 1 year and 0.5° coordinate; 77 events within 6 months and 1° coordinate (about 111 km radius); 94 events within 1 year and 1° coordinate. Their MEM spectral analysis depicted in Fig. 12B confirms the power spectrum depicted in Fig. 4. In particular, note the large 50- to 60-year and 20-year spectral peaks.

References

- Benesty J, Chen J, Huang Y (2006) Estimation of the coherence function with the MVDR approach. *Acoustics, speech and signal processing. ICASSP 2006 proceedings vol 3*, pp. 500–503, doi: [10.1109/ICASSP.2006.1660700](https://doi.org/10.1109/ICASSP.2006.1660700). http://www.mathworks.com/matlabcentral/fileexchange/9781-coherence-function/content/coherence_MVDR
- Bhattacharya P, Chakrabarti BK, Kamal, Samanta D (2009) Fractal models of earthquake dynamics. In: Heinz Georg Schuster (ed) *Reviews of nonlinear dynamics and complexity*, vol 2. Wiley-VCH, Weinheim, pp 107–150 ISBN 3527408509
- Bollinger L, Perrier F, Avouac JP, Sapkota S, Gautam U, Tiwari DR (2007) Seasonal modulation of seismicity in the Himalaya of Nepal. *Geophys Res Lett* 34:L08304. doi:[10.1029/2006GL029192](https://doi.org/10.1029/2006GL029192)
- Carter GC, Knapp C, Nuttall AH (1973) Estimation of the magnitude-squared coherence function via overlapped fast Fourier transform processing. *IEEE Trans Audio Electroacoust* 21:331–344
- Chen L, Chen JG, Xu QH (2012) Correlations between solid tides and worldwide earthquakes $MS \geq 7.0$ since 1900. *Nat Hazards Earth Syst Sci* 12:587–590
- Chylek P, Folland CK, Dijkstra HA, Lesins G, Dubey MK (2011) Ice-core data evidence for a prominent near 20 year time-scale of the Atlantic Multidecadal Oscillation. *Geophys Res Lett* 38:L13704
- Choi DR, Maslov L (2010) Earthquakes and solar activity cycles. *New Concept Global Tectonics Newslett* 57:85–97
- Choi DR, Tsunoda F (2011) Volcanic and seismic activities during the solar hibernation periods. *New Concept Global Tectonics Newslett* 61:78–87
- Choi DR (2013) Earthquakes/volcanic activities and solar cycles. *Global climate status report (GCSR)*. Edition 3–2013, 10–19
- Cochran ES, Vidale JE, Tanaka S (2004) Earth tides can trigger shallow thrust fault earthquakes. *Science* 306:1164–1166

- Davis JC, Bohling G (2001) The search for patterns in ice-core temperature curves. In: Gerhard LC, Harrison WE, Hanson BM (eds) Geological perspectives of global climate change, pp. 213–229
- Forbes RJ (1966) Studies in ancient technology, volume 7 ancient geology: ancient mining and quarrying: ancient mining techniques. (Brill, ISBN13: 9789004006270)
- Enzi S, Bertolin C, Diodato N (2014) Snowfall time-series reconstruction in Italy over the last 300 years. Holocene. doi:10.1177/0959683613518590
- Gao SS, Silver PG, Linde AT, Sacks IS (2000) Annual modulation of triggered seismicity following the 1992 Landers earthquake in California. *Nature* 406:500–504
- Ghil M, Allen RM, Dettinger MD, Ide K, Kondrashov D, Mann ME, Robertson A, Saunders A, Tian Y, Varadi F, Yiou P (2002) Advanced spectral methods for climatic time series. *Rev Geophys* 40:3.1–3.41 (SSA-MTM tool kit for spectral analysis)
- Gipson JM, Ma CP (1998) Site displacement due to variation in Earth rotation. *J Geophys Res* 103:7337–7350
- Gutenberg B, Richter CF (1954) Seismicity of the Earth and Associated Phenomena, 2nd edn. Princeton University Press, Princeton, NJ
- Heki K (2003) Snow load and seasonal variation of earthquake occurrence in Japan. *Earth Planet. Sci. Lett.* 207:159–164
- Ide S, Tanaka Y (2014) Controls on plate motion by oscillating tidal stress: Evidence from deep tremors in western Japan. *Geophys Res Lett* 41:3842–3850
- Jevrejeva S, Moore JC, Grinsted A, Woodworth P (2008) Recent global sea level acceleration started over 200 years ago? *Geophys Res Lett* 35:L08715
- Kilston S, Knopoff L (1983) Lunar-solar periodicities of large earthquakes in southern California. *Nature* 304:21–25
- Klyashtorin L, Lyubushin A (2007) Cyclic climate changes and fish productivity. VNIRO (All Russian Institute Fisheries and Oceanography) Publishing, Moscow, p 224
- Klyashtorin LB, Borisov V, Lyubushin A (2009) Cyclic changes of climate and major commercial stocks of the Barents Sea. *Mar. Biol. Res.* 5:4–17
- Knopoff L (1964) Earth tides as a triggering mechanism for earthquakes. *Bull. seism. Soc. Am.* 54:1865–1870
- Knudsen MF, Seidenkrantz M-S, Jacobsen BH, Kuijpers A (2011) Tracking the Atlantic Multidecadal Oscillation through the last 8,000 years. *Nat. Commun.* 2:178
- Liu C-C, Linde AT, Sacks IS (2009) Slow earthquakes triggered by typhoons. *Nature* 459:833–836
- Loehle C, Scafetta N (2011) Climate change attribution using empirical decomposition of climatic data. *Open Atmos. Sci. J.* 5:74–86
- Lopes RMC, Malin SRC, Mazzarella A, Palumbo A (1990) Lunar and solar triggering of earthquakes. *Phys. Earth Planet. Inter.* 59:127–129
- Luttrell K, Sandwell D (2010) Ocean loading effects on stress at near shore plate boundary fault systems. *Journal of Geophysical Research-Solid Earth.* 115:B08411
- Manzi V, Gennari R, Lugli S, Roveri M, Scafetta N, Schreiber C (2012) High-frequency cyclicity in the Mediterranean Messinian evaporites: evidence for solar-lunar climate forcing. *J. Sed. Res.* 82:991–1005
- Mazzarella A, Palumbo A (1988) Solar, geomagnetic and seismic activity. *Il Nuovo Cimento* 11C:353–364
- Mazzarella A, Palumbo A (1989) Does the solar cycle modulate seismic and volcanic activity? *J. Volc. Geoth. Res.* 39:89–93
- Mazzarella A (2013) Time-integrated North Atlantic Oscillation as a proxy for climatic change. *Natural Science* 5:149–155
- Mazzarella A, Scafetta N (2012) Evidences for a quasi 60-year North Atlantic Oscillation since 1700 and its meaning for global climate change. *Theor. Appl. Climatol.* 107(3–4):599–609
- Mazzarella A, Giuliani A, Scafetta N (2013) Quantifying the Multivariate ENSO Index (MEI) coupling to CO₂ concentration and to the length of day variations. *Theor. Appl. Climatol.* 111:601–607
- McGuire B (2013) *Waking the Giant: How a changing climate triggers earthquakes, tsunamis, and volcanoes.* Oxford University Press, Oxford
- Mignan A, Woessner J (2012) Estimating the magnitude of completeness in earthquake catalogs, Community Online Resource for Statistical Seismicity Analysis, doi:10.5078/corssa-00180805. Available at <http://www.corssa.org>
- Miller SA (2008) Note on rain-triggered earthquakes and their dependence on karst geology. *Geophys. J. Int.* 173:334–338
- Mogi K (1979) Global variation of seismic activity. *Tectonophysics* 57:T43–T50
- Mörner N-M (1989) Global changes: the lithosphere: internal processes and Earth's dynamicity in view of Quaternary observational data. *Quaternary Int.* 2:55–61

- Mörner N-M (1998) New trends in global tectonics. *Phys. Chem. Earth.* 23:825–830
- Mörner N-M (2013) Planetary beat and solar-terrestrial responses. *Pattern Recogn. Phys.* 1:107–116
- Panza GF, Peresan A, Zuccolo E (2011) Climatic modulation of seismicity in the Alpine-Himalayan mountain ranges. *Terra Nova* 23:19–25
- Pagli C, Sigmundsson F (2008) Will present day glacier retreat increase volcanic activity? Stress induced by recent glacier retreat and its effect on magmatism at the Vatnajökull ice cap. Iceland. *Iceland* 35:L09304. doi:[10.1029/2008GL033510](https://doi.org/10.1029/2008GL033510)
- Plinius Secundus C (Pliny the Elder), A.D. 77–79. *Natural History, Book II: cosmology, astronomy and meteorology*
- Qian W-H, Lu B (2010) Periodic oscillations in millennial global-mean temperature and their causes. *Chin. Sci. Bull.* 55:4052–4057
- Ogurtsov MG, Nagovitsyn YA, Kocharov GE, Jungner H (2002) Long-period cycles of the sun’s activity recorded in direct solar data and proxies. *Sol. Phys.* 211:371–394
- Ohtake M, Nakahara H (1999) Seasonality of Great Earthquake Occurrence at the Northwestern Margin of the Philippine Sea Plate. *Pure appl. geophys.* 155:689–700
- Ostřihanský L (2012) Earth’s rotation variations and earthquakes 2010–2011. *Solid Earth Discuss.* 4:33–130
- Riguzzi F, Panza G, Varga P, Doglioni C (2010) Can Earth’s rotation and tidal despinning drive plate tectonics? *Tectonophysics* 484:60–73
- Saar MO, Manga M (2003) Seismicity induced by seasonal groundwater recharge at Mt. Hood, Oregon. *Earth Planet. Sci. Lett.*, 214, 605–618. *Acoustics, Speech and Signal Processing* 3:985–988
- Santamaria I, Via J (2007) Estimation of the Magnitude Squared Coherence Spectrum Based on Reduced-Rank Canonical Coordinates
- Scafetta N, Grigolini P (2002) Scaling detection in time series: diffusion entropy analysis. *Physical Review E* 66:036130
- Scafetta N, West BJ (2004a) Multi-scaling comparative analysis of time series and a discussion on ‘earthquake conversations’ in California. *Physical Review Letters* 92:138501
- Scafetta N, Grigolini P, Imholt T, Roberts JA, West BJ (2004b) Solar turbulence in earth’s global and regional temperature anomalies. *Physical Review E* 69:026303
- Scafetta N, West BJ (2004c) Complexity, multiresolution, non-stationarity and entropic scaling: Teen birth thermodynamics. *Journal of Mathematical Sociology* 28:229–259
- Scafetta N (2010a) *Fractal and Diffusion Entropy Analysis of Time Series - Theory, concepts, applications and computer codes for studying fractal noises and Levy signals.* (VDM Verlag Dr. Muller, 2010)
- Scafetta N (2010b) Empirical evidence for a celestial origin of the climate oscillations and its implications. *J Atmos Solar-Terr Phys* 72:951–970
- Scafetta N (2012a) A shared frequency set between the historical mid-latitude aurora records and the global surface temperature. *J. Atmos. Solar-Terrestr. Phys.* 74:145–163
- Scafetta N (2012b) Multi-scale harmonic model for solar and climate cyclical variation throughout the holocene based on Jupiter-Saturn tidal frequencies plus the 11-year solar dynamo cycle. *J. Atmos. Solar-Terrestr. Phys.* 80:296–311
- Scafetta N (2012c) Does the Sun work as a nuclear fusion amplifier of planetary tidal forcing? A proposal for a physical mechanism based on the mass-luminosity relation. *J. Atmos. Solar-Terrestr. Phys.* 81–82:27–40
- Scafetta N, Humlum O, Solheim J-E, Stordahl K (2013) Comment on “The influence of planetary attractions on the solar tachocline” by Callebaut, de Jager and Duhau. *J. Atmos. Solar-Terrestr. Phys.* 102:368–371
- Scafetta N (2013b) Discussion on climate oscillations: CMIP5 general circulation models versus a semi-empirical harmonic model based on astronomical cycles. *Earth-Science Reviews* 126:321–357
- Scafetta N (2014a) Multi-scale dynamical analysis (MSDA) of sea level records versus PDO, AMO, and NAO indexes. *Clim Dyn* 43:175–192
- Scafetta N (2014b) The complex planetary synchronization structure of the solar system. *Pattern Recognition in Physics* 2:1–19
- Scafetta N (2014c) Discussion on the spectral coherence between planetary, solar and climate oscillations: a reply to some critiques. *Astrophys. Space Sci.* 354:275–299
- Scafetta N, Willson RC (2013) Planetary harmonics in the historical Hungarian aurora record (1523–1960). *Planetary and Space Science* 78:38–44. doi:[10.1016/j.pss.2013.01.005](https://doi.org/10.1016/j.pss.2013.01.005)
- Stephenson FR, Morrison LV (1995) Long-term fluctuations in Earth’s rotation: 700 BC to AD 1990. *Philos Trans A* 351:165–202
- van Stiphout T, Zhuang J, Marsan D (2012) Seismicity declustering. Community online resource for statistical seismicity analysis. doi:[10.5078/corssa-52382934](https://doi.org/10.5078/corssa-52382934)

- Tanaka Y (2014) An approximately 9-year-period variation in seismicity and crustal deformation near the Japan Trench and a consideration of its origin. *Geophys J Int* 196:760–787
- Wang Q-L, Chen Y-T, Cui D-X, Wang W-P, Liang W-F (2000) Decadal correlation between crustal deformation and variation in length of day of the earth. *Earth Planets Space* 52:989–992
- Wang Z, Wu D, Song X, Chen X, Nicholls S (2012) Sun-moon gravitation-induced wave characteristics and climate variation. *J Geophys Res* 117:D07102
- Welch PD (1967) The use of the fast fourier transform for the estimation of power spectra: a method based on time averaging over short, modified periodograms. *IEEE Trans Audio Electroacoust* 15:70–73
- Wu P, Johnston P (2000) Can deglaciation trigger earthquakes in N. America? *Geophys Res Lett* 27(9):1323–1326
- Wyatt M, Curry J (2013) Role of Eurasian Arctic shelf sea ice in a secularly varying hemispheric climate signal during the twentieth century. *Clim Dyn*, doi:[10.1007/s00382-013-1950-2](https://doi.org/10.1007/s00382-013-1950-2)